Biosensors and Bioelectronics 138 (2019) 111313

Contents lists available at ScienceDirect

Biosensors and Bioelectronics

journal homepage: www.elsevier.com/locate/bios

Electrocatalysis of cerium metal-organic frameworks for ratiometric electrochemical detection of telomerase activity

Pengfei Dong[a,b], Longyi Zhu[b], Jing Huang[b], Jujie Ren[a,*], Jianping Lei[b,**]

[a] School of Science, Hebei University of Science and Technology, Shijiazhuang, Hebei, 050018, China
[b] State Key Laboratory of Analytical Chemistry for Life Science, School of Chemistry and Chemical Engineering, Nanjing University, Nanjing, 210023, China

ARTICLE INFO

Keywords:
Electrocatalysis
Biosensors
Metal-organic frameworks
Telomerase
Signal transduction

ABSTRACT

A ratiometric electrochemical biosensor was constructed to detect telomerase activity based on electrocatalysis of cerium-based metal-organic frameworks (CeMOFs) and conformation switch of hairpin DNA. First, the CeMOFs were synthesized using Ce as nodes and 1,3,5-benzenetricarboxylic acid as linker in a green method, and then functionalized with gold nanoparticles. The resulted Au@CeMOF tags demonstrated an excellent electrocatalysis toward hydroquinone oxidation. Meanwhile, a methylene blue (MB) modified hairpin probe was designed with telomerase primer (TP) hybridized "stem" and immobilized on the electrode surface via Au–S chemistry. In the presence of the dNTPs and telomerase, the extended TP can open the hairpin DNA and keep the MB away from the electrode surface, resulting in a decrease of electrochemical signal. In the meantime, the TP-extended part could capture the Au@CeMOF-cDNA tags on the electrode surface via hybridization, leading to the increase electrochemical signal of hydroquinone oxidation catalyzed by Au@CeMOF-cDNA tags. Thus, a ratiometric signal output mode was developed for the electrochemical detection of telomerase activity. This biosensor showed wide dynamic correlation of telomerase activity from 2×10^2 to 2×10^6 cells mL^{-1} with the limit of detection of 27 cells mL^{-1}, and was applied to evaluate telomerase activity in single cell. The ratiometric electrochemical strategy based on the catalysis of MOFs provides a new avenue on signal transduction in telomerase detection.

1. Introduction

Telomerase is a ribonucleoprotein that has a capacity to catalyze the telomere end $(TTAGGG)_n$ sequence for maintaining the proper length and stability of telomeres during cell division. Moreover, telomerase as a marker and therapeutic target is important for the diagnosis and treatment of tumor cells (Zhu et al., 2018). In the past few decades, researchers developed a number of methods for detecting telomerase activity, such as colorimetry (Wang et al., 2018b; Zhang et al., 2016a), fluorescence (Ding et al., 2010; 2016; Ou et al., 2019; Yang et al., 2019), electrochemiluminescence (Wang et al., 2018a), and electrochemical detection (Li et al., 2018; Liu et al., 2016; Ma et al., 2018; Sharon et al., 2010; Wang et al., 2019), coupling with the biotechnological cycling amplification (Gao et al., 2016; Tian et al., 2013; Tian and Weizmann, 2012; Zhang et al., 2016b) and nanomaterial signal amplification (Ling et al., 2016a; 2016b; Lv et al., 2018; Zhou et al., 2016). In particular, electrochemical detection methods are widely concerned by researchers because of their rapid response, low cost, and high sensitivity. For instance, Yi et al. proposed an electrochemical telomerase biosensor based on a structurally-converted DNA probe with ferrocene (Fc) as an electroactive reporter (Yi et al., 2014). Sensitive electrochemical detection of telomerase activity was also reported using spherical nucleic acid gold nanoparticles triggered mimic-hybridization chain reaction with hexaammineruthenium(III) chloride as tags for dual signal amplification (Wang et al., 2015). These electrochemical methods with the direct signal reporters provide a useful platform for the determination of telomerase. For selective and reliable detection of telomerase activity, it is urgent to seek a new signal transduction to detect the telomerase activity against the complex environment.

With the sizes down to nanometer, metal-organic frameworks (MOFs) are involved in bioanalysis due to tunable pore scale, large surface area, and good thermal stability (Martín-Jimeno et al., 2017; Micheroni et al., 2018; Wang et al., 2012). In particular, the integration of MOFs and nanomaterials such as metal NPs, metal oxide, and carbon-based nanomaterials, is leading to the creation of new multifunctional

* Corresponding author.
** Corresponding author.
E-mail addresses: jujieren@126.com (J. Ren), jpl@nju.edu.cn (J. Lei).

https://doi.org/10.1016/j.bios.2019.05.018
Received 11 March 2019; Received in revised form 30 April 2019; Accepted 8 May 2019
Available online 13 May 2019

composites/hybrids for signal amplification in different fields (Cui et al., 2018; Dhakshinamoorthy et al., 2018; Huang et al., 2017; Koo et al., 2016; Shen et al., 2016). By decorating platinum nanozymes on MOFs, the platinum nanoparticles homogeneously immobilized on MOFs possess high stability and catalase-like activity to facilitate the conversion of H_2O_2 to O_2 for enhanced therapy (Zhang et al., 2018). The electrocatalysis of Pd/porphyrinic metal-organic frameworks (PCN-224) toward $NaBH_4$ oxidation was also used to produce a large electrochemical signal for DNA analysis (Yan et al., 2018). Apparently, the synergetic functionalities of metal nanoparticle/MOF hybrids provide a powerful way for signal transduction in electrochemical biosensors.

Unlike conventional electrochemical sensors based on a single current signal, ratiometric electrochemical biosensors are realized by measuring the ratio of two independent electrochemical signal peaks (Ren et al., 2015; Yuan et al., 2017). Thus, ratiometric electrochemical sensors can effectively reduce background signal with high stability, reliability and reproducibility. Inspired by the electrocatalytic properties of MOFs and conformation switch of hairpin DNA, here, we constructed a ratiometric electrochemical technique based on the catalytic properties of MOFs and the electroactive methylene blue-labeled hairpin DNA (MB-HPs) for rapid and sensitive detection of telomerase activity (Fig. 1). First, the CeMOFs were synthesized using Ce as nodes and 1,3,5-benzenetricarboxylic acid as linker at 60 °C for 1 h, and then sequentially functionalized with gold nanoparticles (AuNPs) and capture DNA to obtain the Au@CeMOF-cDNA electrochemical tags. Meanwhile, a methylene blue (MB) modified hairpin DNA with telomerase primer (TP) hybridized "stem" (MB-HPs-TP) was immobilized on the electrode surface via Au–S chemistry. When the TP is extended in the presence of a mixture of telomerase and deoxynucleotide (dNTPs), the hairpin is opened, resulting the reduced current due to the department of the MB from the electrode surface. Meanwhile, the electrochemical tags were introduced onto the surface of the electrode by hybridization between the capture DNA of Au@CeMOF-cDNA and the extension of the TP, producing a large electrocatalytic signal of hydroquinone (HQ) oxidation to p-benzoquinone (BQ). Therefore, the ratiometric electrochemical biosensor based on electrocatalysis of Ce-MOFs was constructed for selective detection of telomerase activity even in single cell, and provided a new signal transduction for efficiently electrochemical biosensing.

2. Experimental

2.1. Reagents and materials

$Ce(NO_3)_3{\cdot}6H_2O$, 1,3,5-benzenetricarboxylic acid (H_3BTC), 6-mercapto-1-hexanol (MCH), 1-(3-(dimethylamino)propyl)-3-ethylcarbodiimide hydrochloride (EDC, purity ≥98%), 3-[(3-cholamidopropyl)dimethylammonio]-1-propanesulfonic acid (CHAPS), N-hydroxysuccinimide (NHS), and hydroquinone were purchased from Aladdin Chemistry Co., Ltd. (Shanghai, China). Tetrachloroauric acid ($HAuCl_4$) was bought from Macklin Biochemical Co., Ltd. (Shanghai, China). HeLa, U87, MCF-7, and HEpG2 cells were from KeyGen Biotech. Co. Ltd. (Nanjing. China). Human telomerase (TE) ELISA kit was from Qiaodu Biotechnology Co. Ltd. (Shanghai, China). Ultrapure water was obtained from a Millipore water purification system (Milli-Q, ≥18.2 MΩ cm), which was used throughout the experiments. All DNA oligonucleotides used in the experiments, the deoxynucleotide solution mixture (dNTPs) and dithiothreitol (DTT) were supplied by Sangon Inc. (Shanghai, China). The sequences of DNA oligonucleotides are as follows:

Hairpin DNA: 5′-MB-AGGGTTTTTTTTTTTTTTTTTTTTTTTTTTTTTTTTTTTAA CCCTAACTCTGCTCGACGGATTTTTTTTTTTTTT–SH–3′

Capture DNA (cDNA): 5′–NH_2–AACCCTAACCCTAACCCT-3′

TP: AATCCGTCGAGCAGAGTT

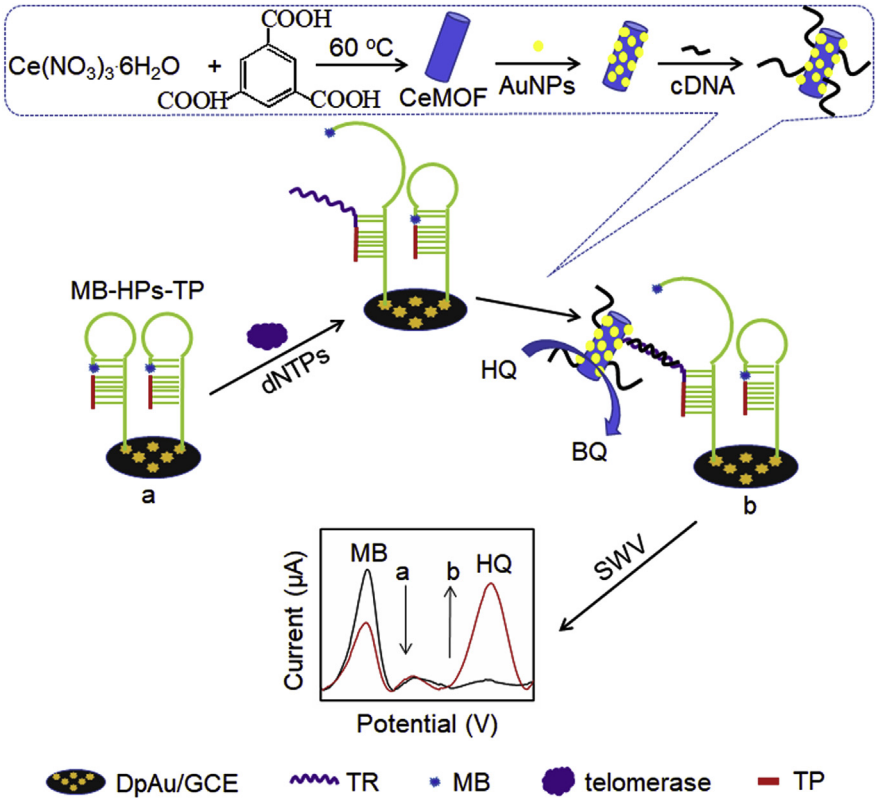

Fig. 1. Schematic illustration of the ratiometric electrochemical strategy based on catalysis of Au@CeMOF toward HQ oxidation and conformation switch of MB-labeled hairpin DNA for detection of telomerase activity.

2.2. Apparatus

Scanning electron microscopy (SEM) and transmission electron microscopy (TEM) images were taken on an S-4800 scanning electron microscope (Hitachi, Japan) and JEM-2010 transmission electron microscope (JEOL, Japan), respectively. Nitrogen isotherms (Micromeritics Tristar 3020) were applied to characterize the structure of CeMOF. X-ray diffraction (XRD) using a Cu sealed tube (λ = 1.54178 Å) at 40 kV and 40 mA. X-ray photoelectron spectroscopy (XPS) was carried out using an ESCALAB 250 spectrometer (Thermo-VG Scientific Co., U.S.A.) with ultra-high vacuum generators. The infrared and UV–vis spectra were obtained on a Vector 22 Fourier transform infrared (FT-IR) spectrometer (Bruker Optics, Germany) and a UV-3600 UV–vis–NIR spectrophotometer (Shimadzu Co., Japan), respectively. Cyclic voltammetry (CV) and square wave voltammetry (SWV) on the CHI660D electrochemical workstation (Shanghai CH Instruments, China) used a three-electrode system composing of a glassy carbon electrode (GCE) as working electrode, Ag/AgCl as reference electrode and platinum wire as auxiliary electrode.

2.3. Synthesis of CeMOF and Au@CeMOF-cDNA

CeMOF was prepared according to previous report with some modification (Xiong et al., 2015). Briefly, 0.434 g $Ce(NO_3)_3{\cdot}6H_2O$ (1.0 mM) was dissolved in 15 mL ultrapure water, and then mixed with 0.23 g H_3BTC (1.0 mM) in 10 mL ultrapure water-ethanol solution (v/v = 1:1) under vigorous stirring. This mixture was kept in water bath at 60 °C for 1 h. By centrifugation and rinsing with ultrapure water and ethanol followed by drying at 80 °C for 10 h, the white product of CeMOF was obtained. The AuNPs functionalized CeMOF composite (Au@CeMOF) was further prepared by mixing 4.0 mL of the prepared AuNPs solution with 2.0 mL of 1.0 mg mL^{-1} CeMOF, and then stirred vigorously for 4 h. The obtained Au@CeMOF was collected by centrifugation and washing with ultrapure water for three times, and redispersed in 1.0 mL of 0.1 M phosphate buffer saline (PBS), pH 7.4.

Au@CeMOF-cDNA was prepared via amide reaction between the –COOH group of Au@CeMOF and the $–NH_2$ group of cDNA. 200 μL of Au@CeMOF aqueous solution (1.0 mg mL^{-1}) was added to 500 μL of 400 mM EDC and 100 mM NHS in ultrapure water with gentle shaking for 2 h. Then, the mixture was centrifuged and washed to remove unbound EDC and NHS. Subsequently, an aqueous DNA solution (10 μM. 0.5 mL) was poured into the above aqueous solution and reacted at room temperature for 4 h. Finally, the unbound DNA was removed by centrifuged at 10000 rpm and washed with water three times. The resulting Au@CeMOF-cDNA conjugate was resuspended in 0.1 M PBS (pH 7.4).

2.4. Cell culture and extraction of telomerase

HeLa cells were cultured with Dulbecco's modified Eagle's medium (DMEM, GIBCO) supplemented with 10% FBS at 37 °C in a humidified atmosphere containing 5% CO_2. The number of cells was determined using a cell counting plate before each experiment. Extraction of telomerase was realized using the universal CHAPS method (Herbert et al., 2006). In brief, 1×10^6 cells were placed in a 1.5 mL centrifuge tube and washed twice with ice-cold PBS (0.1 M pH 7.4) by centrifugation at 2000 rpm for 5 min at 4 °C. The mixture was added to 200 μL of CHAPS Lysis Solution, and pipetted until the cells are evenly dispersed. The solution was incubated in an ice bath for 30 min and then centrifuged at 16000 r/min for 20 min at 4 °C before carefully transferred to a new tube without disturbing the pellet and freezing at −80 °C or use immediately. For the control experiment, the telomerase extract was heat treated at 95 °C for 10 min prior to detection.

2.5. Preparation of MB-HPs-TP probe

Initially, 6 μL of 100 μM MB-HPs was mixed with 8 μL of 100 mM DTT buffer solution and stood for 2 h. Then, the solution was ultrafiltered three times through an ultrafiltration tube (3 KD), and diluted to 3 μM with 10 mM PBS (pH 7.4). Subsequently, the mixture was added with 3 μM TP in an equal volume and kept in a 90 °C water bath for 5 min followed by gradually cooling to room temperature to obtain an MB-HPs-TP probe.

2.6. Polyacrylamide hydrogel electrophoresis (PAGE)

The 15% native PAGE was prepared using 1 × Tris-Borate-EDTA (TBE) buffer. The loading sample was mixed with 7 μL DNA sample and 1.5 μL × 3 loading buffer. The gel was injected in 1 × TBE buffer and carried out at 100 V for 70 min. After dyeing with 4S Green Plus Nucleic Acid Stain for 30 min, the gel was scanned with Molecular Imager Gel Doc XR (BIO-RAD, USA).

2.7. Electrochemical detection of telomerase activity

Before the experiment, GCE was polished by continuous suspension with 1.0 and 0.05 μm alumina suspension, followed by continuous sonication with pure water and ethanol. Subsequently, the clean GCE was electrodeposited with 1% $HAuCl_4$ under a potential of −0.2 V for 30 s to obtain the gold nanoparticles modified electrode (DpAu/GCE). And then 10 μL of MB-HPs-TP (3 μM) was dropped onto the modified electrode for 3 h through Au–S affinity. The electrode was further incubated with 1.0 mM of MCH for 2 h and rinsed with 0.1 M PBS (pH 7.4).

For telomerase extension reaction, the pretreated GCE was immersed in 20 μL of extension solution containing 10 μL of telomerase extract and 2 mM of dNTPs mixture in 1 × TRAP buffer, containing 20 mM Tris-HCl (pH 8.3), 1.5 mM $MgCl_2$, 63 mM KCl, 0.005% Tween-20, 1 mM EGTA and 0.1 mg mL^{-1} BSA. The mixture was incubated at 37 °C for 90 min to allow the extension reaction by telomerase. Then, 10 μL of Au@CeMOF-cDNA was dip-coated onto the pretreated GCE and kept at 37 °C for 90 min. Subsequently, the modified electrode was placed in a PBS (0.1 M, pH 7.4) for SWV from −0.5 V to 0.5 V.

3. Results and discussion

3.1. Characterizations of Au@CeMOF-cDNA tags

The Au@CeMOF-cDNA electrochemical tags were established by sequential functionalizing the pre-synthesized CeMOF with AuNPs and capture DNA. The size and morphology of the products were examined by SEM and TEM measurements. As shown in Fig. 2A, CeMOFs had a rod structure with an average size of about 450 nm in length. Moreover, Au@CeMOF had a rougher surface morphology than that of CeMOF (Fig. 2B–C), and many AuNPs with a diameter of about 6 nm were immobilized on the surface of Au@CeMOF (Fig. 2D). The XRD pattern of the prepared CeMOF showed peaks at 13.4°, 17.5°, 19.3°, 20.7°, and 24.9° (Fig. 2E), indicating the monoclinic, space group *Cc* of crystal structure, which is consistent with previous reports in the literature (Liu et al., 2010; Xiong et al., 2015). Meanwhile, the minor diffraction peak of Au (1 1 1) plane was observed at 44.7° in Au@CeMOF complex (Tu et al., 2009). The FT-IR spectra of both CeMOF and Au@CeMOF exhibited characteristic peaks of the framework structure at 1612-1373 cm^{-1}, 1111 cm^{-1} and 531 cm^{-1} (Fig. 2F), which were attributed to the asymmetric and symmetric stretching-vibration of carboxylate groups and stretching-vibration of Ce–O bond, respectively. High resolution TEM mapping revealed that Ce, Au, C, N, O elements were homogeneously distributed throughout the nanorod structure (Fig. 2G). This result indicated that the structure of CeMOF remained stable during synthesis of the Au@CeMOF composite.

In order to further prove the successful synthesis of the Au@CeMOF,

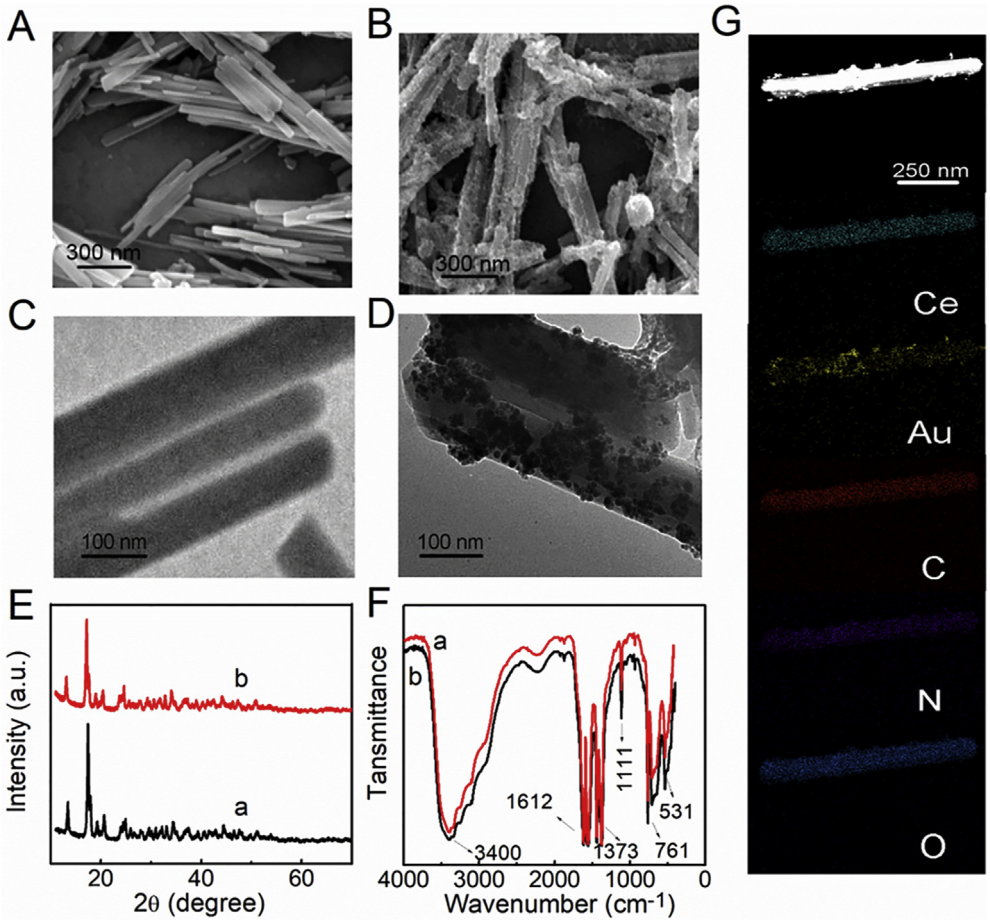

Fig. 2. SEM images of (A) CeMOF and (B) Au@CeMOF, TEM images of (C) CeMOF and (D) Au@CeMOF, (E) XRD patterns and (F) FT-IR of CeMOF (a) and Au@CeMOF (b). (G) High resolution TEM mapping of Au@CeMOF for Ce, Au, C, N, O elements.

XPS was used to analyze elementals of the composite. As shown in Fig. 3A, the XPS spectra of both CeMOF and Au@CeMOF showed peaks of Ce4d (110.07 eV), C1s (285.12 eV), O1s (531.16 eV), and Ce3d (884.12, 903.28 eV). Additional peaks of Au4f (84.2 eV, 87.9 eV), Au4d (333.83 eV, 352.56 eV) were observed for Au@CeMOF, which belonged to the characteristic peaks of AuNPs (Fig. 3A, inset). On the other hand, the intensity of Ce3d (884.12, 903.28 eV) peak for Au@CeMOF was slightly weaker than that of CeMOF, indicating that the Ce signal was partially blocked due to adsorption of AuNPs on the surface of CeMOF (Fig. 3A) during the formation of Au@CeMOF.

Then the capture DNA was conjugated on the surface of Au@CeMOF though amide bonds to obtain Au@CeMOF-cDNA electrochemical tags. The UV–vis spectra showed the characteristic peaks of AuNPs and DNA were at 537 nm and 260 nm, respectively. The prepared Au@CeMOF-cDNA composite exhibited both peaks of AuNPs and cDNA (Fig. 3B). This result was further confirmed by Zeta potential results. After modification with cDNA, the prepared Au@CeMOF-cDNA tags showed a more negative state compared to that of Au@CeMOF (Fig. 3C). In addition, the N_2 adsorption-desorption isotherm distribution showed the surface area of Brunauer-Emmett-Teller of CeMOF was 24.3 m^2/g while the surface area of Au@CeMOF was slightly decreased (Fig. 3D). The above data suggested that the Au@CeMOF-cDNA tag was successfully synthesized.

3.2. Feasibility of the sensor

In order to investigated the feasibility of the sensor, the SWV responses of electrodes with different modifications and treatments were studied under 0.1 M PBS (pH 7.4) containing 20 μM HQ. As shown in Fig. 4A, the electrode of MCH/MB-HPs-TP/DpAu/GCE exhibited an oxidation peak at about −0.29 V (curve a), which was attributed to the signal of electroactive MB on the stem of DNA hairpin structure at the electrode surface. When incubated with inactivated telomerase in the presence of dNTPs, the electrode showed no decrease of the MB peak (curve b). Whereas, after incubation with active telomerase in the presence of dNTPs, a significant decrease in MB peak was observed (curve c), indicating that telomerase has extended the TP and opened the hairpin DNA, led to the department of MB away from the electrode surface and reduction of the electrochemical signal. When the CeMOF-cDNA was added to the telomerase-pretreated electrode for a period of time, the oxidation peak of HQ was emerged at about +0.28 V with the decrease of MB oxidation peak (curve d), indicating that CeMOF was the active site during electrocatalysis. Interestingly, when the Au@-CeMOF-cDNA was used as electrochemical tag instead of CeMOF-cDNA, the HQ peak became much stronger, and MB peak kept constant (curve e), indicating that the AuNPs functionalized CeMOF was more efficient for catalyzing oxidation of HQ. Therefore, the ratiometric electrochemical biosensor was efficiently constructed based on telomerase triggered DNA conformation switch with electrocatalysis of CeMOFs.

The principle of the detection strategy was verified by PAGE (Fig. 4B). MB-HPs-TP complex was obtained by successful hybridization between TP (lane a) and MB-HPs (lane b), showing a slower band (lane c) comparing with the two individual strands. When added inactive telomerase to MB-HPs-TP containing dNTPs (lane e), no additional bands appeared due to non-elongation of TP. After incubation of cDNA (lane d) with MB-HPs-TP, none additional bands appeared as well (lane f), indicating no hybridization happened between MB-HPs-TP and cDNA. Whereas adding active telomerase to the mixture of cDNA and

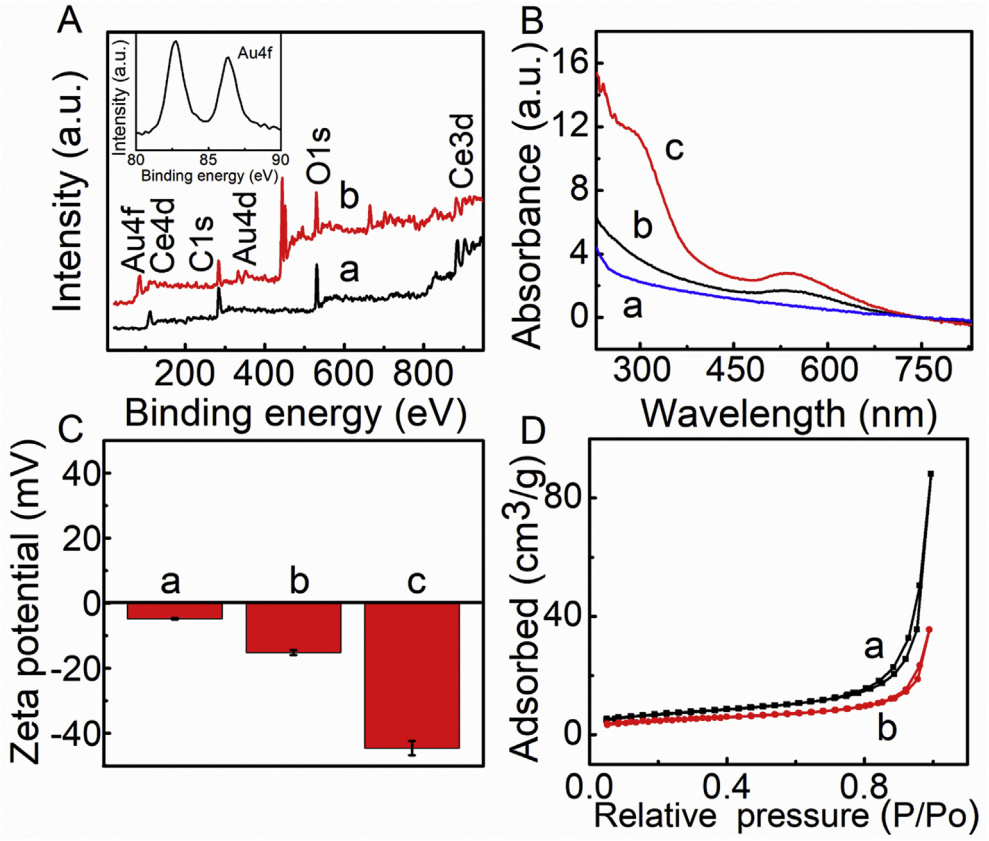

Fig. 3. (A) XPS of CeMOF (a) and Au@CeMOF (b). Inset: XPS of AuNPs. (B) UV–vis spectra of CeMOF (a), Au@CeMOF (b), and Au@CeMOF-cDNA (c). (C) Zeta potentials of AuNPs (a), Au@CeMOF (b), and Au@CeMOF-cDNA (c). (D) N_2 adsorption – desorption isotherm curves of CeMOF (a), and Au@CeMOF (b) at 77 K.

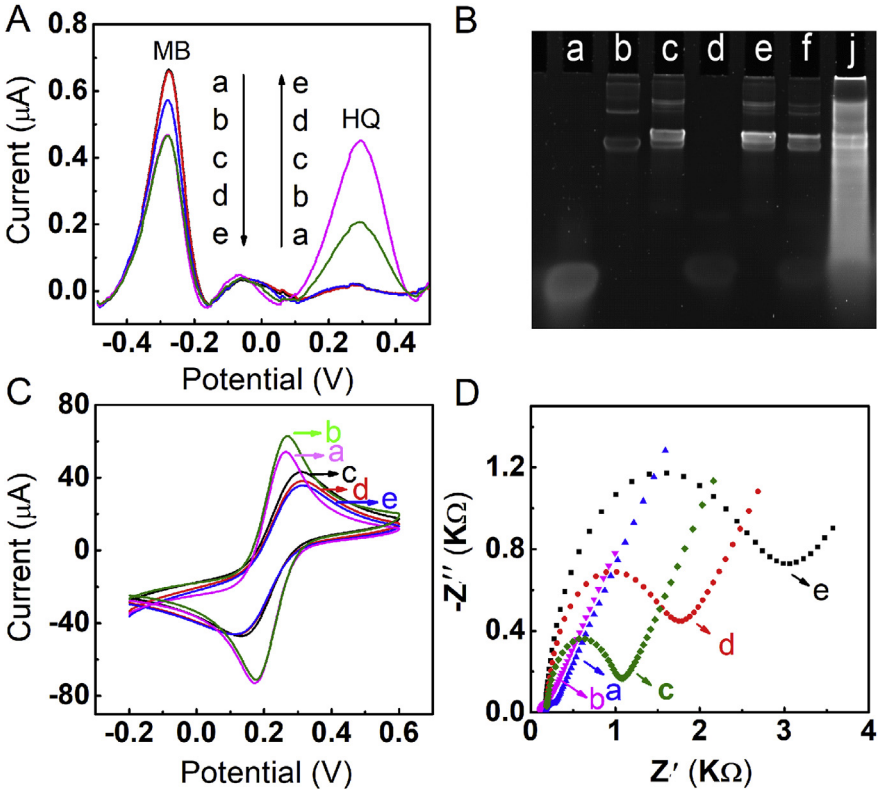

Fig. 4. (A) SWV responses of MB-HPs-TP modified DpAu/GCE electrodes in 0.1 M PBS (pH 7.4) containing 20 μM HQ before (a) and after incubation with heated cell extract (b), and cell extract in presence of dNTPs (c), and followed with CeMOF-cDNA (d) and Au@CeMOF-cDNA (e). (B) PAGE analysis of 2 μM TP (lane a), HP (lane b), MB-HPs-TP (lane c), cDNA (lane d), MB-HPs-TP + the heated extract + dNTPs (lane e), MB-HPs-TS + cDNA (lane f) and MB-HPs-TP + cell extract + cDNA + dNTPs (lane j). (C) CV and (D) EIS response of the electrode interface during the different modification process in the solution containing 5.0 mM $[Fe(CN)_6]^{3-/4-}$ as redox probe: bare GCE (a), DPAu/GCE (b), MB-HPs-TP/DPAu/GCE (c), MCH/MB-HPs-TP/DPAu/GCE before (d) and after (e) incubation with cell extract and dNTPs in the presence of cDNA.

MB-HPs-TP in the presence of dNTPs, a series of bright bands were observed in (lane j), which could be attributed to that TP was extended by telomerase and sequentially hybridized with cDNA. These results successfully demonstrated telomerase-triggered DNA conformation switch and conjugation of cDNA with MB-HPs-TP.

CV and electrochemical impedance spectra (EIS) were further used for characterization of the response and modification process of the electrochemical biosensors. The diameter of the semicircular portion of the EIS corresponds to the interface electron transfer resistance (R_{et}). As shown in Fig. 4C and D, bare GCE (curve a) caused an increase in CV current and a decrease in EIS signal after electrodeposition of AuNPs (curve b). Upon modification of MB-HPs-TP on electrodeposited AuNPs, the CV signal was significantly reduced and the R_{et} increased (curve c). Further blocking the electrode with MCH caused the hindrance of electronic conduction on the electrode surface, which led to the CV signal decrease and the R_{et} increase further (curve d). When telomerase and cDNA were added to the prepared electrode, the CV signal decreased and the R_{et} increased (curve e). These phenomena were attributed to the extension of TP in the presence of dNTPs and telomerase followed by hybridization of the cDNA with the extension of TS. Thereby, the electron transfer on the electrode surface was hindered, which caused the decrease of CV signal and the increase of impedance value. The consistent responses of CV and EIS signals successfully demonstrated the telomerase-triggered assembly on the electrode surface.

3.3. Optimization of detection conditions

In order to achieve the better performance of the biosensor, the experimental conditions of the detection system were optimized by using the peak current ratio of SWV signals responses (I_{HQ}/I_{MB}) versus the observed variables. The density of MB-HPs-TP on the surface of DpAu/GCE electrode will greatly affect the efficacy of the sensor, so the concentration of MB-HPs-TP was optimized. As shown in Fig. 5A, I_{HQ}/I_{MB} increased along with the increase of MB-HPs-TP concentration and reached a maximum value at 3.0 μM. Since the active sites on the electrode surface would be blocked at the higher concentration, the decrease of the I_{HQ}/I_{MB} was observed at 3.5 μM MB-HPs-TP. So we chose 3.0 μM as the optimized concentration. Next, the incubation time of MB-HPs-TP was optimized at DpAu/GCE electrode. The value of I_{HQ}/I_{MB} was enhanced as the increase of incubation time, and became stable after 180 min (Fig. 5B), which was chosen as the optimized incubation time of MB-HPs-TP. Furthermore, the incubation time of telomerase was optimized in the presence of dNTPs at MB-HPs-TP/DpAu/GCE electrode. As shown in Fig. 5C, I_{HQ}/I_{MB} reached a maximum value at 90 min, so the incubation time for telomerase was 90 min. For generation of sufficient signal responses, the incubation time of the Au@CeMOF-cDNA tags was also investigated. The value of I_{HQ}/I_{MB} reached a maximum at 80 min, and then I_{HQ}/I_{MB} slightly weakened, which may be attributed to that the exceed Au@CeMOF-cDNA would hinder the electron transfer at the electrode surface. So, 80 min was chosen as optimal incubation time for Au@CeMOF-cDNA (Fig. 5D).

3.4. Electrochemical detection of telomerase activity

Under optimal conditions, different concentrations of telomerase were introduced to the MCH/MB-HPs-TP/DpAu/GCE electrochemical sensor. As shown in Fig. 6A, the SWV peaks of MB decreased and HQ peaks increased as the increase of telomerase concentrations, oppositely, which could be contributed to the introduction of Au@CeMOF-cDNA tags to the electrode surface and but the department for MB after elongation of telomerase. The responses of the biosensor to cell number were quantified by the SWV peak currents of MB and HQ at −0.29 V and +0.28 V, respectively (Fig. 6B). Then the linear relationship of I_{HQ}/I_{MB} to the logarithm of cell number was plotted, with linear range from 2×10^2 to 2×10^6 HeLa cells mL^{-1} (Fig. 6B, inset). The regression equation is: I (μA) = 0.30 Log(cell number) - 0.35. The limit of detection is 27 HeLa cells mL^{-1} (S/N = 3). This ratiometric method demonstrated the good performance such as a wide linear range and a low limit of detection in detection of telomerase activity comparing with previously reported methods (He et al., 2018; Wang et al., 2019; Xu et al., 2017; Yang et al., 2017).

To evaluate the potential application of the proposed biosensor, the

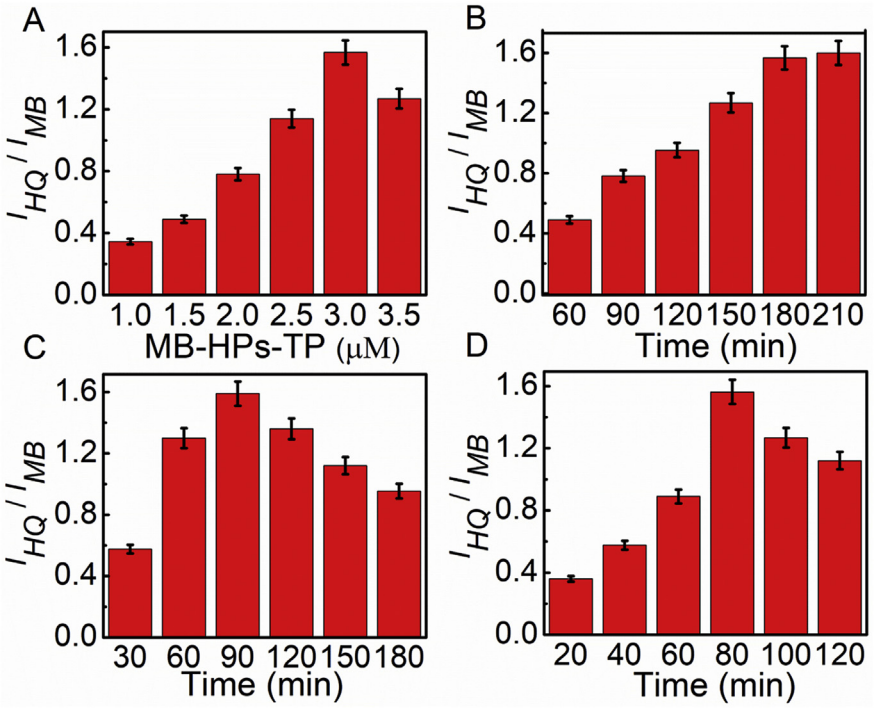

Fig. 5. Effects of (A) concentration and (B) incubation time of MB-HPs-TP, (C) incubation time for telomerase extension reaction and (D) hybridization reaction time between Au@CeMOF-cDNA and the extended TP on the ratiometric current response to telomerase activity of 2×10^6 cells mL^{-1}.

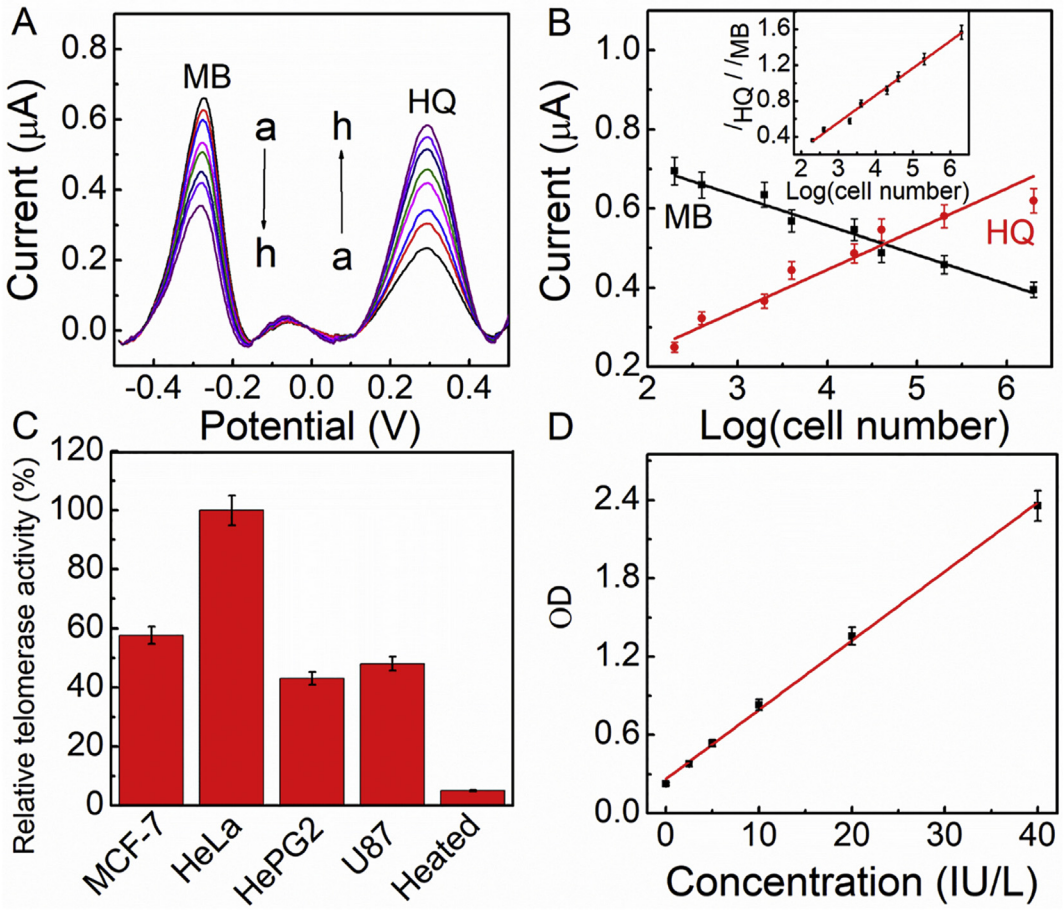

Fig. 6. (A) SWV responses to different HeLa cell numbers in the range of 2×10^2, 4×10^2, 2×10^3, 4×10^3, 2×10^4, 4×10^4, 2×10^5, 2×10^6. (B) Plots of the MB and HQ peak currents as a function of the logarithm of HeLa cell numbers. Inset: Dependence of I_{HQ}/I_{MB} on logarithmic HeLa cell numbers. (C) Analysis of telomerase activities in different cell lines. All the cell extracts were equivalent to 2000 cells mL^{-1}. (D) Standard telomerase activity using a human telomerase ELISA Kit. Error bars indicate standard deviation of triplicate tests.

recovery test was further analyzed with standard telomerase samples in the cell lysate. The test results showed that the recovery rate was 93.8%–107.4%, indicating the acceptable feasibility of the proposed method. After storage for two weeks in a refrigerator at 4 °C, the biosensor maintained at 92.4% of the original value, indicating satisfactory stability of the developed biosensor.

In order to prove the reliability of the ratiometric sensor for telomerase detection, the designed electrochemical biosensor was applied to other cancer cell. As shown in Fig. 6C, HeLa cell extract has the highest telomerase activity compared to that of MCF-7, HepG2 and U87 cells detected by the ratiometric biosensor, which was consistent with previously reported results (Ling et al., 2016a, 2016b; Wu et al., 2014). However, heated HeLa cells showed little signal response due to the lack of telomerase activity. Furthermore, telomerase activity in each HeLa cell was measured to be 3.24×10^{-9} IU by using a commercial ELISA Kit to establish a standard curve ranging from 0 to 40 IU/L with standard telomerase samples, indicating good practicality of this biosensor in complex samples.

4. Conclusion

This work developed a ratiometric electrochemical biosensor by integrating the conformation switch of hairpin DNA with the electrocatalysis of functionalized Au@CeMOF for detection of telomerase activity. The Au@CeMOF demonstrated the excellent electrocatalysis towards HQ oxidation due to its unique structure, providing the enhanced current for signal readout. The telomerase-triggered conformation switch of methylene blue labeled hairpin DNA was utilized as efficient signal transduction strategy, which introduced the CeMOF-based tags on the electrode surface, and departed MB away from the electrode surface. Therefore, a ratiometric signal output mode was developed for the electrochemical detection of telomerase activity. This biosensor demonstrated good performance with wide linear range and low limit of detection, and was applied to evaluate telomerase activity in single cell. The ratiometric sensing platform based on the electrocatalysis of MOFs was enzyme-free, low cost and simple operation, providing a new avenue for signal transduction in detection of various biomolecules.

CRediT authorship contribution statement

Pengfei Dong: Writing - original draft, Supervision. **Jujie Ren:** Writing - original draft, Supervision, Investigation. **Jianping Lei:** Writing - original draft, Supervision, Investigation.

Acknowledgments

We gratefully acknowledge National Natural Science Foundation of China (21675084, 21890741), National Key Technologies R&D Program (2016YFC0302500), and Graduate innovation project of Hebei (CXZZSS2018088).

References

Cui, L., Hu, J., Li, C.C., Wang, C.M., Zhang, C.Y., 2018. Biosens. Bioelectron. 122, 168–174.

Dhakshinamoorthy, A., Asiri, A.M., Alvaro, M., Garcia, H., 2018. Green Chem. 20, 86–107.
Ding, C.F., Li, X.L., Ge, Y., Zhang, S.S., 2010. Anal. Chem. 82, 2850–2855.
Ding, C.F., Li, X.Q., Wang, W., Chen, Y.Y., 2016. Biosens. Bioelectron. 83, 102–105.
Gao, Y.F., Xu, J., Li, B.X., Jin, Y., 2016. Biosens. Bioelectron. 81, 415–422.
He, C.T., Liu, Z.J., Wu, Q.L., Zhao, J., Liu, R.Y., Liu, B.H., Zhao, T.T., 2018. ACS Sens. 3, 757–762.
Herbert, B.S., Hochreiter, A.E., Wright, W.E., Shay, J.W., 2006. Nat. Protoc. 1, 1583–1590.
Huang, N., Yuan, S., Drake, H., Yang, X.Y., Pang, J.D., Qin, J.S., Li, J.L., Zhang, Y.M., Wang, Q., Jiang, D.L., Zhou, H.C., 2017. J. Am. Chem. Soc. 139, 18590–18597.
Koo, W.T., Choi, S.J., Kim, S.J., Jang, J.S., Tuller, H.L., Kim, I.D., 2016. J. Am. Chem. Soc. 138, 13431–13437.
Li, C.C., Hu, J., Lu, M.F., Zhang, C.Y., 2018. Biosens. Bioelectron. 122, 51–57.
Ling, P.H., Lei, J.P., Jia, L., Ju, H.X., 2016a. Chem. Commun. 52, 1226–1229.
Ling, P.H., Lei, J.P., Ju, H.X., 2016b. Anal. Chem. 88, 10680–10686.
Liu, K., You, H.P., Jia, G., Zheng, Y.H., Huang, Y.J., Song, Y.H., Yang, M., Zhang, L.H., Zhang, H.J., 2010. Cryst. Growth Des. 10, 790–797.
Liu, X., Wei, M., Liu, Y.J., Lv, B.J., Wei, W., Zhang, Y.J., Liu, S.Q., 2016. Anal. Chem. 88, 8107–8114.
Lv, Y.Q., Chen, S.Y., Shen, Y.F., Ji, J.J., Zhou, Q., Liu, S.Q., Zhang, Y.J., 2018. J. Am. Chem. Soc. 140, 2801–2804.
Ma, F., Wei, S.H., Leng, J.H., Tang, B., Zhang, C.Y., 2018. Chem. Commun. 54, 2483–2486.
Martín-Jimeno, F.J., Suárez-García, F., Paredes, J.I., Enterría, M., Pereira, M.F.R., Martins, J.I., Figueiredo, J.L., Martínez-Alonso, A., Tascón, J.M.D., 2017. ACS Appl. Mater. Interfaces 9, 44740–44755.
Micheroni, D., Lan, G.X., Lin, W.B., 2018. J. Am. Chem. Soc. 140, 15591–15595.
Ou, X.W., Zhan, S.S., Sun, C.L., Cheng, Y., Wang, X.D., Liu, B.F., Zhai, T.Y., Lou, X.D., Xia, F., 2019. Biosens. Bioelectron. 124–125, 199–204.
Ren, K.W., Wu, J., Yan, F., Zhang, Y., Ju, H.X., 2015. Biosens. Bioelectron. 66, 345–349.
Sharon, E., Freeman, R., Riskin, M., Gil, N., Tzfati, Y., Willner, I., 2010. Anal. Chem. 82, 8390–8397.
Shen, W.J., Zhuo, Y., Chai, Y.Q., Yuan, R., 2016. Biosens. Bioelectron. 83, 287–292.
Tian, L.L., Weizmann, Y., 2012. J. Am. Chem. Soc. 135, 1661–1664.
Tian, T., Peng, S., Xiao, H., Zhang, X.E., Guo, S., Wang, S.R., Zhou, X., Liu, S.M., Zhou, X., 2013. Chem. Commun. 49, 2652–2654.
Tu, Y.B., Luo, J.Y., Meng, M., Wang, G., He, J.J., 2009. Int. J. Hydrogen Energy 34, 3743–3754.
Wang, C., Zhang, T., Lin, W.B., 2012. Chem. Rev. 112, 1084–1104.
Wang, C.L., Yang, H.T., Wu, S.S., Liu, Y.J., Wei, W., Zhang, Y.J., Wei, M., Liu, S.Q., 2018a. Trends Anal. Chem. 105, 404–412.
Wang, D.N., Guo, R., Wei, Y.Y., Zhang, Y.Z., Zhao, X.Y., Xu, Z.R., 2018b. Biosens. Bioelectron. 122, 247–253.
Wang, L., Meng, T.J., Yu, G.S., Wu, S.S., Sun, J.J., Jia, H.X., Wang, H., Yang, X.J., Zhang, Y.F., 2019. Biosens. Bioelectron. 124–125, 53–58.
Wang, W.J., Li, J.J., Rui, K., Gai, P.P., Zhang, J.R., Zhu, J.J., 2015. Anal. Chem. 87, 3019–3026.
Wu, L., Wang, J.S., Ren, J.S., Qu, X.G., 2014. Adv. Funct. Mater. 24, 2727–2733.
Xiong, Y.H., Chen, S.H., Ye, F.G., Su, L.J., Zhang, C., Shen, S.F., Zhao, S.L., 2015. Chem. Commun. 51, 4635–4638.
Xu, X.L., Wei, M., Liu, Y.J., Liu, X., Wei, W., Zhang, Y.J., Liu, S.Q., 2017. Biosens. Bioelectron. 87, 600–606.
Yan, T.T., Zhu, L.Y., Ju, H.X., Lei, J.P., 2018. Anal. Chem. 90, 14493–14499.
Yang, H.T., Fu, F.J., Li, W., Wei, W., Zhang, Y.J., Liu, S.Q., 2019. Chem. Sci. 10, 3706–3714.
Yang, H.T., Liu, A.R., Wei, M., Liu, Y.J., Lv, B.J., Wei, W., Zhang, Y.J., Liu, S.Q., 2017. Anal. Chem. 89, 12094–12100.
Yi, Z., Wang, H.B., Chen, K., Gao, Q., Tang, H., Yu, R.Q., Chu, X., 2014. Biosens. Bioelectron. 53, 310–315.
Yuan, Y.H., Chi, B.Z., Wen, S.H., Liang, R.P., Li, Z.M., Qiu, J.D., 2017. Biosens. Bioelectron. 102, 211–216.
Zhang, L., Zhang, S.J., Pan, W., Liang, Q.C., Song, X.Y., 2016a. Biosens. Bioelectron. 77, 144–148.
Zhang, X.F., Cheng, R., Shi, Z.L., Jin, Y., 2016b. Biosens. Bioelectron. 75, 101–107.
Zhang, Y., Wang, F.M., Liu, C.Q., Wang, Z.Z., Kang, L.H., Huang, Y.Y., Dong, K., Ren, J.S., Qu, X.G., 2018. ACS Nano 12, 651–661.
Zhou, Q., Li, G.H., Zhang, Y.J., Zhu, M., Wan, Y.K., Shen, Y.F., 2016. Anal. Chem. 88, 9830–9836.
Zhu, X.L., Ye, H.Y., Liu, J.W., Yu, R.Q., Jiang, J.H., 2018. Anal. Chem. 90, 13188–13192.